

Applications

Julia Vettermann*, Alexander Steinert, Christian Brecher, Peter Benner and Jens Saak

Compact thermo-mechanical models for the fast simulation of machine tools with nonlinear component behavior

Kompakte thermomechanische Modelle für die schnelle Simulation von Werkzeugmaschinen mit nichtlinearem Komponentenverhalten

<https://doi.org/10.1515/auto-2022-0029>

Received February 24, 2022; accepted July 7, 2022

Abstract: In this contribution, advanced modeling of thermo-mechanical effects in machine tools with nonlinear machine components is investigated using the example of a feed axis. Strategies of model order reduction for this coupled thermo-mechanical model with nonlinear subsystem are presented. Numerical investigations of the performance of the resulting reduced-order model compared to the original one conclude this article.

Keywords: thermo-mechanical model, machine tool, model order reduction, nonlinear subsystem

Zusammenfassung: In diesem Beitrag wird die erweiterte Modellierung thermomechanischer Effekte in Werkzeugmaschinen mit nichtlinearen Maschinenkomponenten am Beispiel einer Vorschubachse untersucht. Es werden Strategien zur Modellordnungsreduktion für dieses gekoppelte thermomechanische Modell mit nichtlinearem Teilsystem vorgestellt. Numerische Untersuchungen der Leistungsfähigkeit des resultierenden Modells reduzierter Ordnung im Vergleich zum ursprünglichen Modell schließen den Artikel ab.

***Corresponding author: Julia Vettermann**, Faculty of Mathematics, Technische Universität Chemnitz, Reichenhainer Straße 39/41, 09126 Chemnitz, Germany, e-mail:

julia.vettermann@mathematik.tu-chemnitz.de

Alexander Steinert, Christian Brecher, Laboratory for Machine Tools and Production Engineering (WZL), RWTH Aachen University, Steinbachstraße 19, 52074 Aachen, Germany, e-mails:

a.steinert@wzl.rwth-aachen.de, c.brecher@wzl.rwth-aachen.de

Peter Benner, Jens Saak, Computational Methods in Systems and Control Theory, Max Planck Institute for Dynamics of Complex Technical Systems, Sandtorstraße 1, 39106 Magdeburg, Germany, e-mails: benner@mpi-magdeburg.mpg.de,

saak@mpi-magdeburg.mpg.de

Schlagwörter: thermomechanisches Modell, Werkzeugmaschine, Modellordnungsreduktion, nichtlineares Teilsystem

1 Introduction

Machine tools are permanently exposed to complex static, dynamic and thermal loads. An undesirable displacement of the tool center point (TCP) limiting the achievable work piece quality at given productivity is the consequence. The technical complexity of machine tools requires advanced modeling approaches to describe static, dynamic and thermal effects accurately, since both machine structural parts and machine components affect the overall behavior.

The finite element method (FEM) is a powerful and vastly used tool to model static, dynamic and thermal effects in machine tools, which is reflected in a wide range of scientific work in this field. Yet, current research impulses in the context of model-based data analytics strive for process parallel solutions processing machine internal data [1]. In order to combine existing modeling capabilities with modern data-driven approaches, a massive reduction of calculation times is a fundamental requirement. At this point, model order reduction (MOR) becomes crucial. Sophisticated MOR strategies enable the computation of compact low-dimensional models for fast simulations of entire machine tool models while preserving a certain model accuracy.

Within the scope of this paper, a thermo-mechanical FE model of a feed axis is set up. As integral part of a modern 5-axis machine tool, this assembly group includes the relevant characteristics of machine tools mentioned above. Nonlinear boundary conditions, which are challenging in the field of MOR, are considered. Furthermore, novel preprocessing techniques allow classic linear MOR to be applied and, thus, enable for drastically reduced

computing times. Transient thermo-mechanical interactions of the feed axis are calculated in a final investigation.

2 Modeling of coupled thermo-mechanical systems

2.1 Thermo-mechanical behavior of machine tools

To date, the areas of thermal [2, 3, 4] and mechanical [5, 6] simulation have been widely studied. For subsystems like the main spindle unit, interactions between both thermal and mechanical domain were investigated and respective simulation models were derived [7].

For a body of homogeneous and temporally constant material properties (density ρ , heat capacity c_p and conductivity λ), the thermal behavior can be expressed analytically, resulting in a partial differential equation for the temperature field T (1). Here, the external thermal load \dot{q} (heat flux density) has a spatial (δ) and temporal (t) dependency, where δ denotes the three-dimensional position coordinates,

$$\rho c_p \frac{\partial}{\partial t} T - \lambda \nabla(\nabla T) = \dot{q}(\delta, t). \quad (1)$$

Elastostatic equilibrium for solid bodies can be expressed by Navier-Cauchy equation

$$(\lambda + \mu) \nabla(\nabla \delta) + \mu \nabla^2 \delta = -F. \quad (2)$$

Again, constant material parameters (Lamé parameters λ and μ) are considered and F represents a volume-distributed force. Although we restrict our considerations

to constant material parameters, the approach is not limited to this assumption. Note that in the case of variable parameters methods of MOR for parameter-varying systems, see [8], would have to be applied to (21) in Sec. 3.2.

Combined thermo-elastic behavior of solid bodies is often assumed to be linear. Although machine tools mainly consist of large structural parts, machine components like bearings, linear guideways or ball screws represent functionally relevant elements that usually act as coupling elements between the structural parts. Due to their nonlinear mechanical characteristics, thermal expansion of structural parts, for example, may affect mechanical conditions in machine components as displayed in Fig. 1.

In general, machine components act as significant heat sources in thermally sensitive regions of a machine tool. While bearings of the main spindle, for example, are characterized by the installation in structures of high power density, linear guideways induce heat along large structural parts that significantly contribute to the overall TCP error [9]. In reaction, transient temperature fields cause thermal expansion and thermal stress that ultimately result in reactive forces. These forces, in turn, influence contact pressings in machine components affecting their frictional behavior that initially caused the heat generation.

In order to investigate the effects of cross-domain behavior, an FE-based coupled model for a feed axis of a 5-axis machine tool is designed (Fig. 2).

Besides two structural parts ($P1$ and $P2$) that represent the slide and the headstock, the assembly group contains two linear guideways, arranged in parallel, with two carriages each, i. e. four machine components in total (C_1 to C_4). While the structural parts are modeled via FEM, the components are represented as spring damper elements with nonlinear, load-dependent characteristics. A more detailed description is given below.

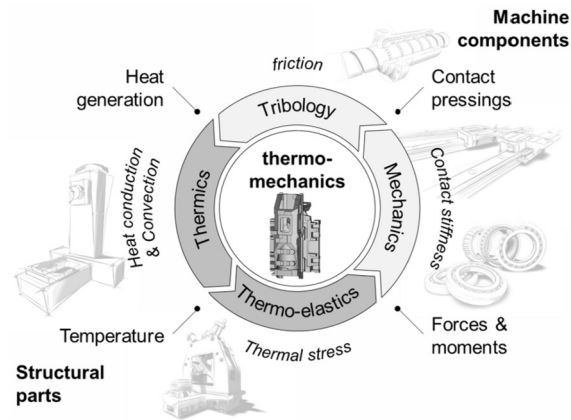


Figure 1: Closed loop of thermo-mechanical interactions in machine tools.

2.2 Modeling of structural parts

The given thermo-elastic partial differential equations in (1) and (2) are solved numerically. By discretizing in space and time, for each structural part of the assembly, a matrix equation

$$(\mathbf{C}^P + dt \cdot \mathbf{K}^P) \Theta_t^P = \mathbf{C}^P \cdot \Theta_{t-1}^P + dt \cdot \mathbf{B}^P u_t, \quad (3)$$

with $\mathbf{B}^P u_t$ denoting the external influences on the system, can be derived.

Here, the heat capacity matrix \mathbf{C}^P only contains non-zero entries for thermal degrees of freedom (DOFs). In con-

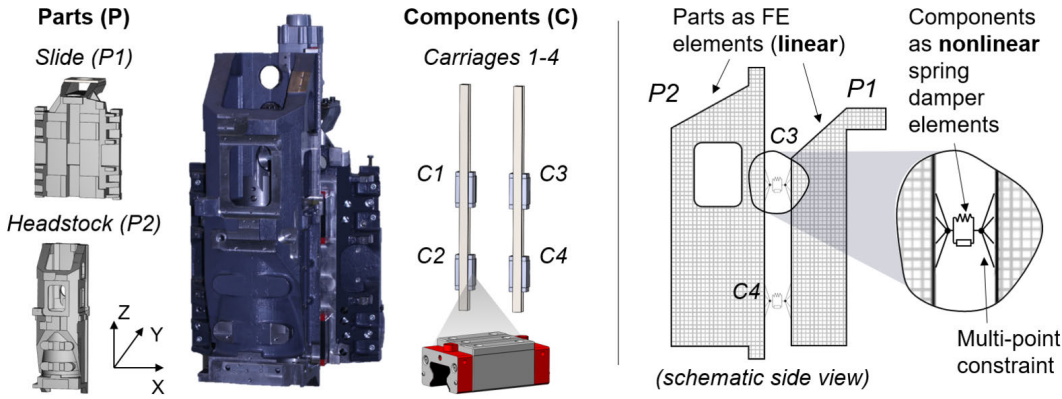


Figure 2: Feed axis of a modern 5-axis vertical milling machine.

trast, the matrix \mathbf{K}^P is composed of a thermal heat conduction part \mathbf{K}_{th}^P , an elastic stiffness part \mathbf{K}_{el}^P and a part considering thermal elongation $\mathbf{K}_{el,th}^P$. Due to the different time scales of the thermal and mechanical system, dynamic effects in the mechanical part are negligible. Thus, the mechanical system is modeled as static, and also the coupling from elastic to thermal degrees of freedom is neglected, in this paper. The resulting structure of each system matrix is visualized in Fig. 3, highlighting the asymmetric structure.

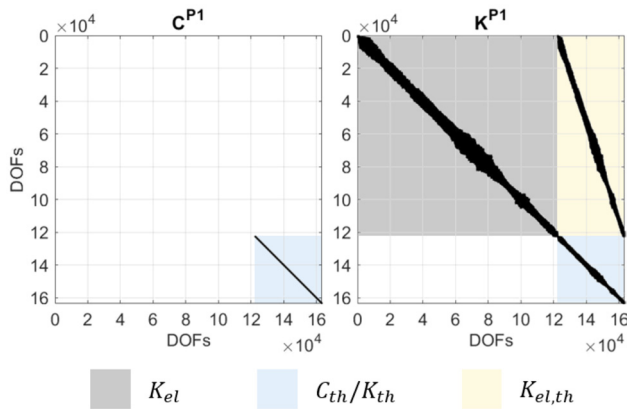


Figure 3: System matrices \mathbf{C}^{P1} and \mathbf{K}^{P1} .

The machine structure is meshed with tetrahedral, quadratic SOLID227 coupled-field elements using ANSYS. As a result, for each node four DOFs

$$\Theta^P = [\Delta^P \quad T^P]^T = [\delta_x \quad \delta_y \quad \delta_z \quad T]^T \quad (4)$$

follow. The vector Θ^P contains structural DOFs Δ^P (translatory displacements δ in x-, y-, and z-direction) and one thermal DOF T^P (nodal temperature).

2.3 Modeling of machine components

On the one hand, linear guideways are designed to ensure backlash- and friction-free motion in feed direction (z-direction in Fig. 2). On the other hand, the other DOFs except the linear feed direction are supposed to be locked. Since dynamic effects are not considered in this paper, linear guideways are modeled as nonlinear spring elements with 7 DOFs

$$\begin{aligned} \Theta^c &= [\Delta^c \quad \phi^c \quad T^c]^T \\ &= [\delta_x \quad \delta_y \quad \delta_z \quad \varphi_x \quad \varphi_y \quad \varphi_z \quad T]^T. \end{aligned} \quad (5)$$

In addition to the considered DOFs for structural parts (4), Θ^c does also contain respective rotations φ around all three coordinate axes in ϕ^c .

Since the stiffness matrix

$$\mathbf{K}^c = \begin{bmatrix} K_{\delta_x \delta_x} & \cdots & \mathbf{0} & \mathbf{0} \\ \vdots & \ddots & \mathbf{0} & \mathbf{0} \\ \mathbf{0} & \mathbf{0} & K_{\varphi_z \varphi_z} & \mathbf{0} \\ \mathbf{0} & \mathbf{0} & \mathbf{0} & K_T \end{bmatrix} \quad (6)$$

refers to the geometric center, only direct stiffness entries on the main diagonal are included.

The scalar entries $K_{\delta_x \delta_x}$ to K_T represent mechanical elasticity and thermal heat conductivity of the respective machine component. Since these values depend on the conditions in each rolling contact inside the component, they are updated explicitly based on previous calculation results. In general, contact stiffness can be calculated analytically, with Hertzian theory [10], based on the relative positioning of the contact partners to each other. Furthermore, the equilibrium of external forces and internal contact forces of each roller element is calculated iteratively in each time step. In [11], respective analytic-numerical models for machine components like linear guideways, ball

screws and bearings were developed. Based on these existing models, the nonlinear behavior of the components is calculated a priori for different operating points and provided in tables. Explicitly calculated nonlinear stiffness of guideways can be expressed as follows:

$$\mathbf{K}_t^c = f(\Theta_{t-1}^c); \quad \Theta_{t-1}^c = f(\mathbf{K}_{t-1}^c, F_{t-1}, T_{t-1}). \quad (7)$$

One spring element of seven DOFs connects two so-called condensation nodes of same dimension each. Thus, the resulting stiffness matrix describing one machine component has the dimension 14×14 and the structure

$$\mathbf{K}^C = \begin{bmatrix} \mathbf{K}^c & -\mathbf{K}^c \\ -\mathbf{K}^c & \mathbf{K}^c \end{bmatrix}. \quad (8)$$

2.4 General assembly of the coupled system

Based on thermal and mechanical modeling of structural parts and machine components, the coupled system can be assembled. In this procedure, the following steps are performed:

1. Definition of boundary conditions (BC) and couplings between structural parts
2. Formulation of multi-point constraints (MCs)
3. Assembly of coupled system.

In step one, relevant machine components as couplings between structural parts are identified. For each coupling, an initial stiffness matrix and condensation nodes are set up. After that, multi-point constraints connect contact regions on structural parts with previously defined condensation nodes. For this purpose, an RBE3 formulation is used [6]. Based on the principle of virtual work, (9) represents the equations that couple seven DOFs of a condensation node with all N coupling nodes of the associated contact area of the structural part. The formulation for mechanical energy used to couple structural DOFs is therefore expanded to an equivalent thermal formulation containing the heat flux \dot{Q} and temperatures T .

$$\begin{bmatrix} F^c \\ M^c \\ \dot{Q}^c \end{bmatrix} \cdot \begin{bmatrix} \Delta^c \\ \phi^c \\ T^c \end{bmatrix} = \sum_{n=1}^N \left(\begin{bmatrix} F_n^p \\ \dot{Q}_n^p \end{bmatrix} \cdot \begin{bmatrix} \Delta_n^p \\ T_n^p \end{bmatrix} \right). \quad (9)$$

Furthermore, condensation node moments M^C are put in equilibrium with moments coming from coupling forces F_n^P with corresponding lever arms Δ_n^P , expressed as the cross-product

$$M^C = \sum_{n=1}^N (\Delta_n^P \times F_n^P). \quad (10)$$

In matrix notation,

$$\mathbf{L}_{MC} \begin{bmatrix} \Delta^P \\ \Delta^C \end{bmatrix} = 0 \quad (11)$$

provides the connection of condensation and coupling DOFs.

Based on this formulation, the global coupling matrix \mathbf{L} for one structural part and one condensation node to be coupled can be assembled as follows:

$$\mathbf{L} = \begin{bmatrix} \mathbf{I} & 0 & 0 & 0 \\ 0 & \mathbf{I} & 0 & 0 \\ 0 & 0 & -\mathbf{L}_{MC} & 0 \\ 0 & 0 & 0 & \mathbf{I} \end{bmatrix}. \quad (12)$$

By applying dual assembly based on theory of dynamic substructuring [12], the system represented by the uncoupled stiffness matrix \mathbf{K} is coupled by multiplying with the matrix \mathbf{L} from both sides. A priori, \mathbf{K} is assembled by stacking the individual subsystems \mathbf{K}_i^P and \mathbf{K}_j^C diagonally,

$$\mathbf{K}_{\text{coupled}} = \mathbf{L}^T \mathbf{K} \mathbf{L}. \quad (13)$$

Although forces F^C and moments M^C of condensation nodes, as well as coupling forces F^P , were added as additional DOFs to the system of equations, only respective condensation node forces and moments remain, hereinafter referred to as Lagrange multiplier λ . The overall vector of DOFs Θ now consist of structural part DOFs Θ^P , machine component DOFs Θ^C and Lagrange multiplier λ ,

$$\Theta = \begin{bmatrix} \Theta^P \\ \Theta^C \\ \lambda \end{bmatrix} = \begin{bmatrix} \Delta^P \\ T^P \\ \Delta^C \\ \phi^C \\ T^C \\ \lambda \end{bmatrix}. \quad (14)$$

The considered feed axis is composed of two parts and four components. The coupled stiffness matrix is

$$\mathbf{K}_{\text{coupled}} = \begin{bmatrix} \mathbf{K}^{P_i} & 0 & \mathbf{K}^{P_i C_j} \\ 0 & \mathbf{K}^{C_j} & -\mathbf{I} \\ \mathbf{K}^{P_i C_j} & -\mathbf{I} & 0 \end{bmatrix}. \quad (15)$$

Fig. 4 shows the global stiffness matrix with its three different sub-blocks. The first, by far largest block represents part-DOFs with constant entries. The second block with condensation-DOFs contains variable entries that need to be updated every time step. However, this block

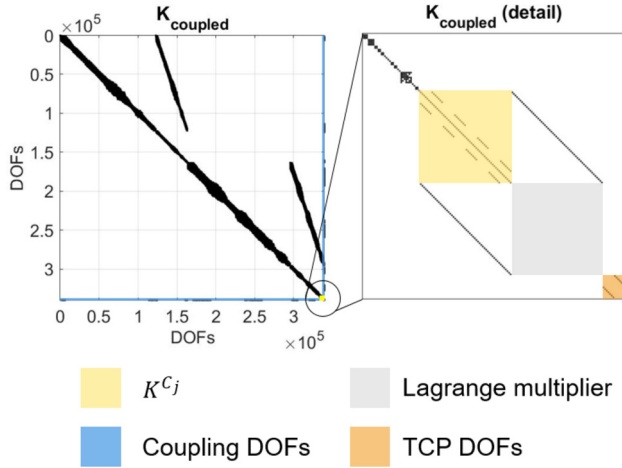


Figure 4: Structure of the coupled stiffness matrix.

Table 1: Overview over all considered DOFs.

2 parts	4 components + TCP	Lagrange multiplier
84,977 nodes	9 condensation nodes	9 condensation nodes
4 DOFs p. node	7 DOFs p. node	7 DOFs p. node
339,908 DOFs	63 DOFs	63 DOFs

only covers 56 DOFs while the assembled model has 340,034 DOFs in total (see Tab. 1). In addition, block three realizes the coupling of part and component blocks. For static assemblies without relative motion, this block is also constant. In case of a relative motion, this block needs to be updated based on the current position of the feed axis. This could be achieved through the discretization of the rails of linear guideways into discrete sections. Then, for each section a multi-point constraint has to be modeled and the corresponding matrix \mathbf{L}_{MC} has to be set up. As a result, a coupling block $\mathbf{K}^{P_i C_j}$ containing connections to respective coupling nodes exists for each rail section and has to be updated position-based within the model.

3 MOR for a coupled system with nonlinear subsystem

MOR aims at finding a low-dimensional surrogate model approximating the high-dimensional dynamical system, which, as in the case at hand, is often obtained by a spatial discretization, e. g. by FEM. Then, the reduced order model (ROM) replaces the original model in applications, where fast and repeated model evaluations are required, such as real-time predictions, optimization or control. In

the scope of this paper, the much smaller ROMs are utilized to speed up the thermo-mechanical simulation of a feed axis.

3.1 MOR for linear time-invariant (LTI) systems

We aim to separate the linear part of the above simulation model and reintegrate a much smaller surrogate into the coupled simulation. Hence, here we consider the representation of a linear time-invariant (LTI) system in generalized state-space form

$$\begin{aligned} \mathbf{E}\dot{\mathbf{x}}(t) &= \mathbf{A}\mathbf{x}(t) + \mathbf{B}u(t), \\ y(t) &= \mathbf{C}\mathbf{x}(t) + \mathbf{D}u(t) \end{aligned} \quad (\Sigma)$$

with constant system matrices $\mathbf{E}, \mathbf{A} \in \mathbb{R}^{n \times n}$, which describe the dynamics of the system, the input map $\mathbf{B} \in \mathbb{R}^{n \times m}$, the output map $\mathbf{C} \in \mathbb{R}^{p \times n}$ and the feedthrough matrix $\mathbf{D} \in \mathbb{R}^{p \times m}$, respectively. The vector $\mathbf{x} \in \mathbb{R}^n$ denotes the state, which includes the DOFs in the considered model and the outputs $\mathbf{y} \in \mathbb{R}^p$ contain values in points of interest, like temperatures in sensor positions or the TCP-displacement. The vector u together with the input map \mathbf{B} describe the external influences on the system, e. g., in our case, the heat fluxes induced to the linear parts from the ambient temperature or the nonlinear components of the machine.

The goal of our projection-based MOR is the computation of truncation matrices $\mathbf{V}, \mathbf{W} \in \mathbb{R}^{n \times r}$, which restricts the model to an r -dimensional subspace with $r \ll n$, while the essential information on the input-to-output dynamics of the system is preserved. The ROM is of the form

$$\begin{aligned} \tilde{\mathbf{E}}\dot{\tilde{\mathbf{x}}}(t) &= \tilde{\mathbf{A}}\tilde{\mathbf{x}}(t) + \tilde{\mathbf{B}}u(t), \\ \tilde{y}(t) &= \tilde{\mathbf{C}}\tilde{\mathbf{x}}(t) + \mathbf{D}u(t) \end{aligned} \quad (\tilde{\Sigma})$$

with the reduced matrices $\tilde{\mathbf{E}} := \mathbf{W}^T \mathbf{E} \mathbf{V}$, $\tilde{\mathbf{A}} := \mathbf{W}^T \mathbf{A} \mathbf{V}$, $\tilde{\mathbf{B}} := \mathbf{W}^T \mathbf{B}$ and $\tilde{\mathbf{C}} := \mathbf{C} \mathbf{V}$, the reduced state $\tilde{\mathbf{x}}(t) \in \mathbb{R}^r$ and the approximated outputs $\tilde{y}(t) \approx y(t) \in \mathbb{R}^p$. The output error $\|y - \tilde{y}\|$ is required to be small in a suitable norm.

There are several well known MOR techniques for LTI systems (Σ), which differ in the way the truncation matrices \mathbf{V} and \mathbf{W} are determined. Besides the energy-based reduction methods, like balanced truncation (BT), which we use to demonstrate our approach in this paper, also methods based on Krylov subspaces, e. g. moment matching techniques and rational interpolation, enjoy great popularity in the field of MOR. Another class of MOR methods are the training-based approaches, which rely on repeated

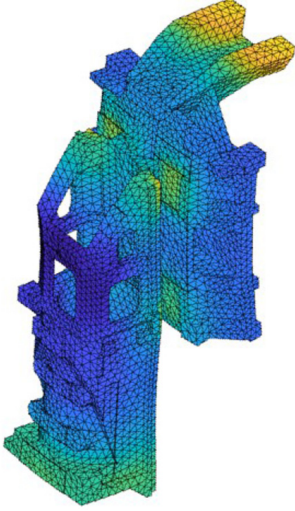


Figure 5: Sketch of the position of the feed axis model used for the simulations.

system simulations, like proper orthogonal decomposition (POD) and reduced basis (RB) methods. More information on the various MOR techniques, especially concerning the basic principles, algorithms, stability and error estimation can be found in, e. g. [13, 14, 15, 16] and the references therein. In principle, all these methods could be used for the reduction of the linear part in our framework.

3.2 MOR for fixed relative positions

We consider the fixed pose in Fig. 5 of the feed axis model described in Section 2. In order to develop a strategy to compute a ROM for this system, we have to analyze, and make use of, the structure. After the spatial discretization by the FEM and the assembly of the coupled system (Section 2.4) we set

$$\begin{aligned} x_1 &= \Theta^P, & x_2 &= \begin{bmatrix} \Theta^C \\ \lambda \end{bmatrix}, \\ \mathbf{A}_{11} &= -\mathbf{K}^P, & \mathbf{A}_{12} &= \begin{bmatrix} \mathbf{0} & -\mathbf{K}^{PC} \end{bmatrix}, \\ \mathbf{A}_{21} &= \begin{bmatrix} \mathbf{0} \\ -\mathbf{K}^{PC} \end{bmatrix}, & \mathbf{A}_{22}(x_2) &= \begin{bmatrix} f(x_2) & -\mathbf{I} \\ -\mathbf{I} & \mathbf{0} \end{bmatrix}, \end{aligned}$$

to obtain the following coupled system Σ in generalized state-space form

$$\begin{aligned} \begin{bmatrix} \mathbf{E}_{11} & \mathbf{0} \\ \mathbf{0} & \mathbf{0} \end{bmatrix} \begin{bmatrix} \dot{x}_1 \\ \dot{x}_2 \end{bmatrix} &= \begin{bmatrix} \mathbf{A}_{11} & \mathbf{A}_{12} \\ \mathbf{A}_{21} & \mathbf{A}_{22} \end{bmatrix} \begin{bmatrix} x_1 \\ x_2 \end{bmatrix} + \begin{bmatrix} \mathbf{B}_1 \\ \mathbf{B}_2 \end{bmatrix} u, \\ y &= \begin{bmatrix} \mathbf{C}_1 & \mathbf{C}_2 \end{bmatrix} \begin{bmatrix} x_1 \\ x_2 \end{bmatrix}. \end{aligned} \quad (16)$$

The system consists of a linear thermo-elastic part Σ_{lin} of dimension n_1 , which is coupled to a nonlinear system Σ_{nl} of dimension n_2 through the coupling matrices \mathbf{A}_{12} and \mathbf{A}_{21} . \mathbf{A}_{22} is the nonlinear subsystem consisting of the stiffness of each linear guide and respective condensation DOFs. Since \mathbf{A}_{22} realizes the coupling of the structural machine parts, it is responsible for relative displacements and rotations of the rigid bodies, on the one hand, and heat exchange between the bodies, on the other hand. In consequence, the impact of flexible bodies is extended by the rigid body behavior. $f(x_2) \in \mathbb{R}^{\frac{n_2}{2} \times \frac{n_2}{2}}$ represents the nonlinear part of the stiffness matrix and equals K^G in (15), which is dependent on the DOFs of the multi-point constraints x_2 . In the simulation this part has to be updated after every time step. Thereby for every component submatrix (one submatrix for each carriage) a factor is calculated, which depends on the difference between the displacement DOFs in x-direction of the respective carriage and a product specific parameter representing the linear guideways. The matrix \mathbf{E}_{11} consists of the heat capacity matrix in the thermal part and zeros in the elastic part, which is considered to be static (see Section 2), and thus \mathbf{E}_{11} is singular.

To achieve an efficient reduction process, the linear and nonlinear parts of the system are separated, in order to treat each with the most appropriate method. This is done by a decomposition of the coupling blocks \mathbf{A}_{12} and \mathbf{A}_{21} in the form $\mathbf{A}_{12} = \mathbf{B}_{\text{lin}} \mathbf{C}_{\text{nl}}$ and $\mathbf{A}_{21} = \mathbf{B}_{\text{nl}} \mathbf{C}_{\text{lin}}$, analogous to [17]. Both can be achieved by the (economy-size) singular value decomposition (SVD). For large sparse matrices, the required subset of singular values and vectors can be computed efficiently, by first determining the structural rank of the matrix and then running the sparse SVD with that number of desired values and vectors. Afterwards the system can be reformulated as an interconnected system [18] with an explicit coupling in the form of additional internal input matrices \mathbf{B}_{lin} , \mathbf{B}_{nl} and output matrices \mathbf{C}_{lin} , \mathbf{C}_{nl} :

$$\Sigma_{\text{lin}} : \begin{cases} \mathbf{E}_{11} \dot{x}_1 = \mathbf{A}_{11} x_1 + \begin{bmatrix} \mathbf{B}_1 & \mathbf{B}_{\text{lin}} \end{bmatrix} \begin{bmatrix} u \\ y_{\text{nl}} \end{bmatrix}, \\ \begin{bmatrix} y_1 \\ y_{\text{lin}} \end{bmatrix} = \begin{bmatrix} \mathbf{C}_1 \\ \mathbf{C}_{\text{lin}} \end{bmatrix} x_1. \end{cases} \quad (17a)$$

$$\Sigma_{\text{nl}} : \begin{cases} \mathbf{0} = \mathbf{A}_{22}(x_2) x_2 + \begin{bmatrix} \mathbf{B}_2 & \mathbf{B}_{\text{nl}} \end{bmatrix} \begin{bmatrix} u \\ y_{\text{lin}} \end{bmatrix}, \\ \begin{bmatrix} y_2 \\ y_{\text{nl}} \end{bmatrix} = \begin{bmatrix} \mathbf{C}_2 \\ \mathbf{C}_{\text{nl}} \end{bmatrix} x_2. \end{cases} \quad (17b)$$

For systems with a large number of coupled DOFs it is recommended to use a low-rank approximation of the coupling blocks [17, Ch. 8], to keep the numbers of inputs and

outputs small, compared to the original system dimension. Systems with many inputs and outputs may require special, numerically more expensive, MOR techniques, e. g. [19], introducing an additional outer approximation step, and consequently additional approximation errors. For a general overview of MOR for coupled dynamical systems, see e. g. [20].

Due to the small dimension of the nonlinear subsystem compared to that of the linear one, we decided to reduce only the linear part and preserve the full nonlinear subsystem. In case the dimension of Σ_{nl} gets too large, suitable techniques for the reduction of nonlinear systems can be found e. g. in [14, Sec. 3], [21] and the references therein.

With a grouping of the states by thermal and elastic degrees of freedom, $x_{th} = T$ and $x_{el} = [\delta_x \ \delta_y \ \delta_z]^T$, and the combined input $u_{el,th} = [u \ y_{nl}]^T$ from external inputs u and internal inputs y_{nl} from the nonlinear subsystem, we can write Σ_{lin} as

$$\begin{bmatrix} \mathbf{0} & \mathbf{0} \\ \mathbf{0} & \mathbf{E}_{th} \end{bmatrix} \begin{bmatrix} \dot{x}_{el} \\ \dot{x}_{th} \end{bmatrix} = \begin{bmatrix} \mathbf{A}_{el} & \mathbf{A}_{el,th} \\ \mathbf{0} & \mathbf{A}_{th} \end{bmatrix} \begin{bmatrix} x_{el} \\ x_{th} \end{bmatrix} + \begin{bmatrix} \mathbf{B}_{el} \\ \mathbf{B}_{th} \end{bmatrix} u_{el,th}, \quad (18)$$

$$y_{el,th} = \mathbf{C}_{el}x_{el} + \mathbf{C}_{th}x_{th}, \quad (19)$$

where the subscripts el and th denote the parts of the elastic and the thermal system and the matrix $\mathbf{A}_{el,th}$ represents the coupling of the temperature field x_{th} in direction of the displacement field x_{el} . Note that the influence of the deformation on the temperature field is considered negligible and, thus, set to the zero matrix $\mathbf{0}$.

This representation takes the form of a semi-explicit differential-algebraic equation (DAE) of index 1 [22, Ch. 5.1], and allows for an index-reduction as it was applied to a thermo-elastic machine tool assembly in [23]. From the first block-row of (18), we get

$$x_{el} = -\mathbf{A}_{el}^{-1}\mathbf{A}_{el,th}x_{th} - \mathbf{A}_{el}^{-1}\mathbf{B}_{el}u_{el,th}. \quad (20)$$

At this point it has to be guaranteed that \mathbf{A}_{el} has to be invertible, which will be addressed in more detail in Sec. 3.3. Inserting (20) into the second block row and the output equation (19) leads to a representation of the same system dynamics by a set of ordinary differential equations together with an updated output equation

$$\begin{aligned} \mathbf{E}_{th}\dot{x}_{th} &= \mathbf{A}_{th}x_{th} + \mathbf{B}_{th}u_{el,th}, \\ y &= \mathbf{C}_{el}(-\mathbf{A}_{el}^{-1}\mathbf{A}_{el,th}x_{th} - \mathbf{A}_{el}^{-1}\mathbf{B}_{el}u_{el,th}) + \mathbf{C}_{th}x_{th} \\ &= (\mathbf{C}_{th} - \mathbf{C}_{el}\mathbf{A}_{el}^{-1}\mathbf{A}_{el,th})x_{th} - \mathbf{C}_{el}\mathbf{A}_{el}^{-1}\mathbf{B}_{el}u_{el,th}. \end{aligned} \quad (21)$$

Now defining $\mathbf{E} = \mathbf{E}_{th}$, $\mathbf{A} = \mathbf{A}_{th}$, $x = x_{th}$, $\mathbf{B} = \mathbf{B}_{th}$, $\mathbf{C} = \mathbf{C}_{th} - \mathbf{C}_{el}\mathbf{A}_{el}^{-1}\mathbf{A}_{el,th}$ and $\mathbf{D} = -\mathbf{C}_{el}\mathbf{A}_{el}^{-1}\mathbf{B}_{el}$, we receive a standard LTI state-space system (Σ). If both thermal and elastic

degrees of freedom use the same mesh and ansatz functions in the FE-formulation and for a three-dimensional problem, as in our case, the system dimension in (21) is already reduced to $\frac{1}{4}$ of the state-dimension in (18), while the information of the elasticity system is completely captured in the output equation of (21). Note that for a two-dimensional problem the system dimension would be reduced to $\frac{1}{3}$ by the index-reduction. Now, we can further reduce (21), which represents the index-reduced formulation of the linear subsystem Σ_{lin} in (17a), using standard MOR methods for LTI systems. Finally, the resulting ROM $\tilde{\Sigma}_{lin}$ is recombined with the nonlinear part Σ_{nl} . Here, special attention has to be drawn to the structure of the new feedthrough matrix \mathbf{D} , since it also contains parts including the artificial internal inputs and outputs, which have to be considered in the newly coupled system. The specific structure of \mathbf{D} can be split into four parts containing the feedthrough for the coupled system, but also describes the influence of the inputs u on the nonlinear states, the interaction of the linear and nonlinear states, as well as the influence of the nonlinear states on the output:

$$\mathbf{D} = \begin{bmatrix} \mathbf{D}_{1,ext} & \mathbf{D}_{1,nl} \\ \mathbf{D}_{lin,ext} & \mathbf{D}_{lin,nl} \end{bmatrix}. \quad (22)$$

Consequently, a reduced coupled system of the form

$$\begin{bmatrix} \tilde{\mathbf{E}}_{11} & \mathbf{0} \\ \mathbf{0} & \mathbf{0} \end{bmatrix} \begin{bmatrix} \dot{\tilde{x}}_1 \\ \dot{\tilde{x}}_2 \end{bmatrix} = \begin{bmatrix} \tilde{\mathbf{A}}_{11} & \tilde{\mathbf{B}}_{lin}\mathbf{C}_{nl} \\ \mathbf{B}_{nl}\tilde{\mathbf{C}}_{lin} & \mathbf{A}_{up} \end{bmatrix} \begin{bmatrix} \tilde{x}_1 \\ x_2 \end{bmatrix} + \begin{bmatrix} \tilde{\mathbf{B}}_1 \\ \mathbf{B}_{up} \end{bmatrix} u, \quad (23)$$

$$\tilde{y} = [\tilde{\mathbf{C}}_1 \quad \mathbf{C}_{up}] \begin{bmatrix} \tilde{x}_1 \\ x_2 \end{bmatrix} + \mathbf{D}_{1,ext}u$$

with the updated matrices

$$\begin{aligned} \mathbf{A}_{up} &= \mathbf{A}_{22}(x_2) + \mathbf{B}_{nl}\mathbf{D}_{lin,nl}\mathbf{C}_{nl}, \\ \mathbf{B}_{up} &= \mathbf{B}_2 + \mathbf{B}_{nl}\mathbf{D}_{lin,ext}, \\ \mathbf{C}_{up} &= \mathbf{C}_2 + \mathbf{D}_{1,nl}\mathbf{C}_{nl} \end{aligned}$$

is obtained.

3.3 Freed rigid body modes

An important fact, which has to be considered in the context of decoupling an interconnected system containing a mechanical part, is the problem of freed rigid body modes. In our case, the nonlinear part of the system represents the carriages, which connect the slide with the headstock. Thus, in the considered use case, decoupling the linear and nonlinear part of the system also leads to 6 rigid body modes in the headstock model.

Due to zero eigenvalues, \mathbf{A}_{el} is not invertible, but the invertibility is a prerequisite for the application of (20). In the following we want to discuss some strategies to tackle this problem.

An obvious idea is a change in the FE-model itself based on an additional fixing of the concerned assemblies. However, this could be disadvantageous due to an excessive stiffness in the FE-model and restrictions in the modeling process.

A second possibility results from a numerical perturbation of the model, leading to a shift of the eigenvalues. We follow this strategy in the numerical experiments in this contribution. To this end, we introduce an ϵ -perturbation of the form $\hat{\mathbf{A}}_{el} = \mathbf{A}_{el} - \epsilon \mathbf{I}$ in (18), analogous to [24], in our case using $\epsilon = 10^{-5}$. In that case we have to condone the loss of error bounds of the MOR method as a drawback.

A third opportunity will be part of future investigations. Here a change from the stationary elasticity model to a dynamic second-order elasticity model including the mass matrix enables the treatment of the rigid body modes as part of MOR methods used in the context of elastic multibody simulation, see [25, 26].

4 Numerical experiments

The model was established in ANSYS and the matrices needed for the representation (16) were exported for the nonlinear simulation and MOR in MATLAB[®]. The FE model consists of 340,034 DOFs, 20 inputs and 63 outputs. The simulated loadcase includes a nodal heat flux at TCP of 50 W, a nodal heat flux of 20 W at each carriage and rail, as well as a surface heat flux of 30 W m^{-2} on the slide, taking the effects of the z-motor into account. The decoupled and index-reduced system (21) was reduced with balanced truncation and the ROM was again coupled with the nonlinear part as described in (23). For the MOR of the linear part we used the BT implementation for large sparse systems, included in the open source MATLAB tool M-M.E.S.S. – the MATLAB Matrix Equation Sparse Solvers [27]. The truncation tolerance and thus the BT error bound was set to 10^{-2} . With that tolerance we obtain a recoupled ROM of the form (23) with a reduced order of 207, in which the nonlinear part is of order 126. Consequently, the linear part of the model was reduced from 339,908 DOFs to 81 reduced DOFs. First we want to have a look at the reduction error for a completely linear simulation ($\mathbf{A}_{22} = \text{const.}$) and afterwards with active nonlinearity ($\mathbf{A}_{22} = \mathbf{A}_{22}(x_2)$). Hence, we

can classify the errors resulting from the reduction process and from the nonlinearity.

Data and code availability

All MATLAB codes for execution of the experiments reported here are available as a code package authored by J. Vettermann, J. Saak and A. Steinert [28]. The data matrices for a test model are provided differing in system dimension and used parameters to the here presented model and thus generating slightly different results.

4.1 Results

The generation of the ROM and all simulations have been executed on a compute server, whose hardware and software specifications are described in Tab. 2, at TU Chemnitz. Since we did not have exclusive access to the machine, timings below are expected to be representative, but may have been affected by other computations on the same machine.

Table 2: Hardware and software environments for the experiments.

CPU	Intel(R) Xeon(R) CPU E7-4880 v2 @ 2.50 GHz
Cores	4×15
RAM	1 TB
OS	Ubuntu 18.04.6 LTS
Platform type	x86_64 (64 Bit)
MATLAB	R2021b
M-M.E.S.S.	2.1 [27]

From a physical point of view, relevant comparison variables are the relative x-displacement between shoes and rails of the linear guideways and the absolute z-displacement of the TCP. While the former effect has significant influence on the component stiffness and thus on the absolute displacement under static load, the latter effect directly affects the achievable working accuracy.

We observe a very good conformity between the results of the original full order model (FOM) and the ROM both in the linear and nonlinear case, as Fig. 6, 7 and 8 show exemplary for the position pictured in Fig. 5. The simulation was executed with the implicit Euler method for a time span of 100 s with a constant time step size of 0.1 s, thus we have a total number of 1,000 time steps. The plots in Fig. 6 and 7 show the errors of the difference between the temperature DOFs as well as the displacement DOFs in x-direction of

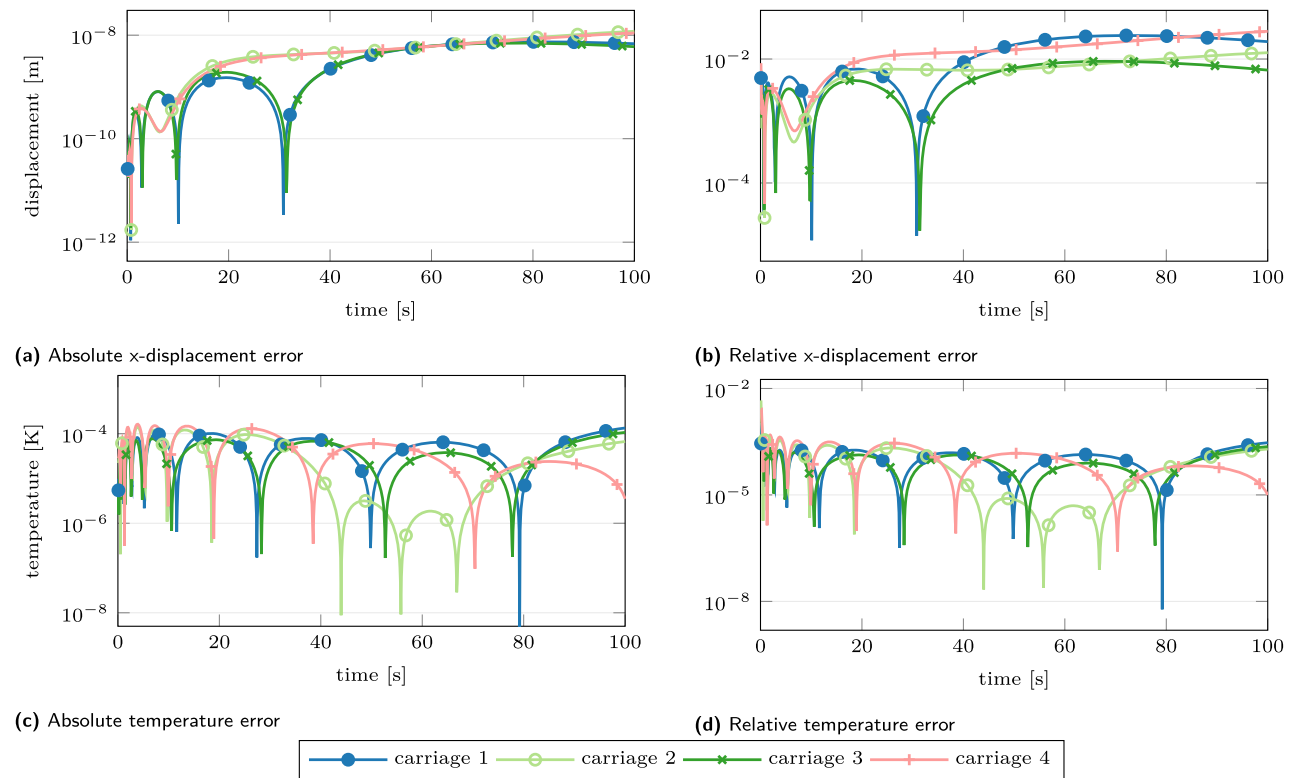


Figure 6: Relative and absolute errors of the relative x-displacement between shoes and rails of the linear guideways and the related temperature difference for the ROM for the fixed position sketched in Fig. 5 simulated as fully linear system.

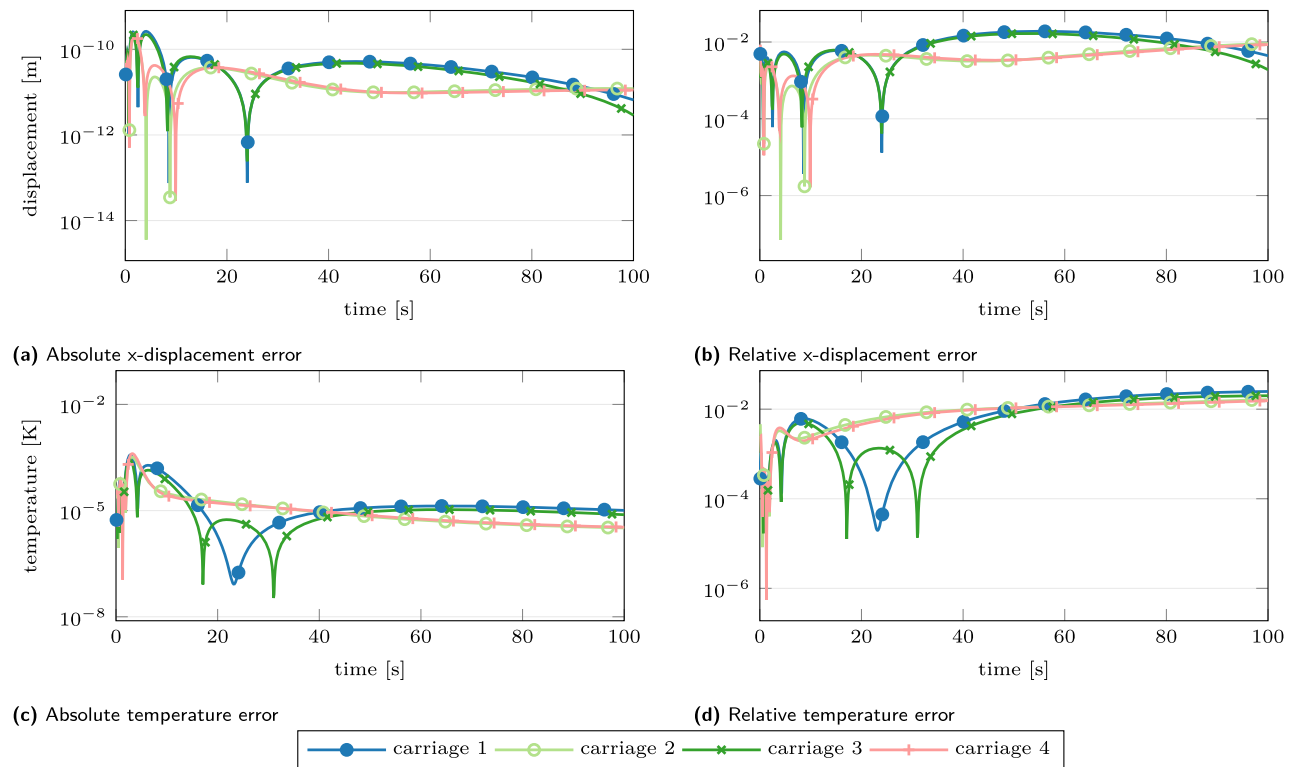


Figure 7: Relative and absolute errors of the relative x-displacement between shoes and rails of the linear guideways and the related temperature difference for the ROM for the fixed position sketched in Fig. 5 simulated with active nonlinearity.

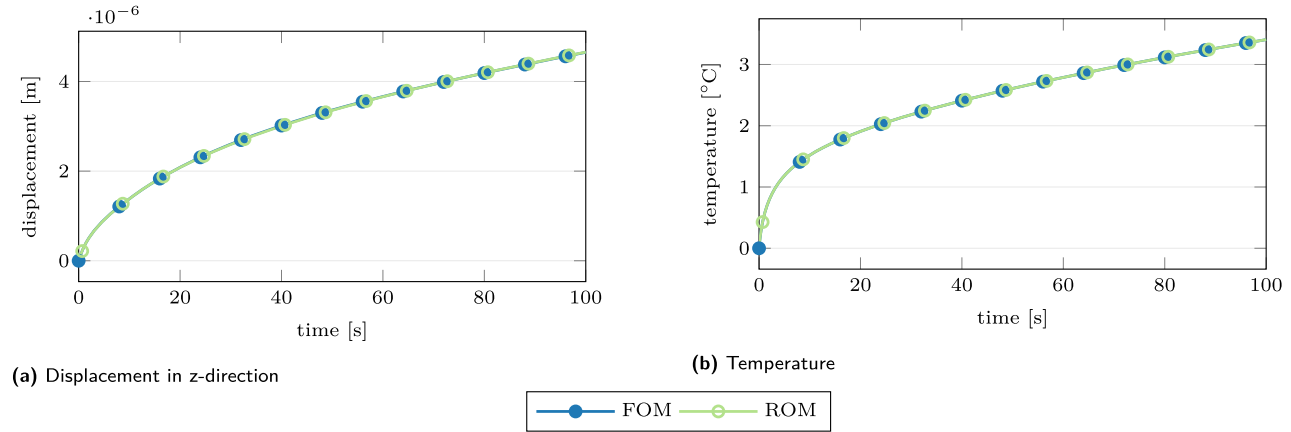


Figure 8: Comparison of the results for the FOM and the ROM at the TCP for the fixed position sketched in Fig. 5 simulated with active nonlinearity.

Table 3: Comparison of reduction and simulation times t_{red} and t_{sim} for the linear (l) and the nonlinear (nl) simulation (time step size: 0.1 s, 1000 time steps).

Model	Size	t_{red}	t_{sim}
FOM, l	340,034	–	835.6 s
ROM, l	207	341.6 s	1.5 s
FOM, nl	340,034	–	140220 s ~ 39 h
ROM, nl	207	341.6 s	3.3 s

the carriages. A good match of these displacement values is of particular importance, due to the fact, that the update of the nonlinear part of the system depends on them. With average relative displacement errors of order 10^{-2} and thus a reduction error smaller than the expected FE-modeling error, the model accuracy is preserved. We aim at a good approximation of the displacement and temperature results in the ROM at our point of interest – the TCP. A reliable approximation especially of the TCP displacement in the ROM is crucial for, e. g. real-time error correction of the thermally induced TCP error during the manufacturing process. As Fig. 8 shows, a very good reproduction of the FOM trajectory with the ROM simulation with a relative error of order 10^{-3} can be achieved for the z-displacement, the temperature results are even better with a relative error of order 10^{-4} .

In Tab. 3 the order of the models as well as the times needed for the reduction and simulation process for the investigated simulation models are summarized. Note that we achieve a speedup of the simulation time in the fully linear case, for FOM and ROM, by the reuse of the LU-decomposition in the linear solver for the step, which is possible due to the linearity of the system and the use of

a constant time step size in the integration step. This explains the large difference between the simulation times for the FOM in the linear and nonlinear cases.

We see that the simulation of the ROM comes up with a formidable speedup of the simulation times compared to the FOM. Even in the case that just one simulation is required, the sum of the time needed for the reduction and simulation process of the ROM is smaller than one simulation cycle of the FOM. Furthermore, a comparison of the storage amount of the FOM and ROM might be an important fact, which plays a major role if a model has to be saved directly on the numerical control system of the machine tool. We can not only observe a drastical reduction of the simulation time, but also of the memory requirements for the ROM. While the FOM needs 212.81 MB, the ROM just requires 0.23 MB.

5 Conclusions

This contribution combines advanced modeling techniques to consider nonlinear component behavior in a classical FE-model and a MOR strategy tailored to the particular needs of the resulting differential-algebraic machine tool model with geometrically local nonlinearities. The numerical investigations showed a drastic reduction of the simulation times achieved by the use of a suitable ROM while preserving a certain model accuracy.

In a further step, an approach to handle the problem of relative movement and thus moving loads in the model will be investigated. For this task a switched system shall be compared to a formulation as a parameter-varying system, see e. g. [23, 29]. Furthermore, the ROM will be used

as surrogate model in different use-cases, for example the computation of transient thermo-mechanical interactions affecting the life time of the feed axis, as well as computations for data driven approaches, e. g. the generation of training data for artificial neural networks.

Funding: Funded by the German Research Foundation – Project-ID 174223256 – TRR 96.

References

- Brecher, C., A. Broos, F. Butz, A. Epple, M. Fey, M. Kaefer, W. Koehler, M. Koenigs, M. Lange, S. Neus, M. Queins, M. Weigold, F. Wellmann, H. Wille and B. Zapf. 2017. *Nutzen und Potenziale modellbasierter Datenanalyse*. Apprimus Verlag, pp. 163–195.
- Großmann, K. and G. Jungnickel. 2010. *Simulation des thermischen Verhaltens von Werkzeugmaschinen*. Adv. Des. Control, addprint AG, Dresden.
- Ess, M. 2012. Simulation and compensation of thermal errors of machine tools. Ph. D. thesis, Institute of Machine Tools and Manufacturing, ETH Zürich. <https://doi.org/10.3929/ethz-a-7357121>.
- Brecher, C., S. Ihlenfeldt, S. Neus, A. Steinert and A. Galant. 2019. Thermal condition monitoring of a motorized milling spindle, *Production Engineering. Res. Dev.* 13(5): 539–546. <https://doi.org/10.1007/s11740-019-00905-3>.
- Altintas, Y., C. Brecher, M. Weck and S. Witt. 2005. Virtual machine tool. *CIRP Ann.* 54(2): 115–138. [https://doi.org/10.1016/S0007-8506\(07\)60022-5](https://doi.org/10.1016/S0007-8506(07)60022-5).
- Brecher, C., M. Fey, C. Tenbrock and M. Daniels. 2016. Multipoint constraints for modeling of machine tool dynamics. *J. Manuf. Sci. Eng.* 138(5). <https://doi.org/10.1115/1.4031771>.
- Brecher, C., A. Steinert, S. Neus and M. Fey. 2020. Metrological investigation and simulation of thermo-mechanical interactions in externally driven spindles. Special Interest Group Meeting: Thermal Issues, pp. 14–17.
- Benner, P., S. Gugercin and K. Willcox. 2015. A survey of projection-based model reduction methods for parametric dynamical systems. *SIAM Rev.* 57(4): 483–531. <https://doi.org/10.1137/130932715>.
- Brecher, C., M. Fey, S. Neus and Y. Shneor. 2014. Influences on the thermal behavior of linear guides and externally driven spindle systems. *Prod. Eng. Res. Dev.* 9(1): 133–141. <https://doi.org/10.1007/s11740-014-0589-0>.
- Harris, T. 2006. *Essential Concepts of Bearing Technology*. CRC Press Inc., Boca Raton.
- Brecher, C., B. Eßer, J. Falker, F. Kneer and M. Fey. 2018. Modelling of ball screw drives rolling element contact characteristics. *CIRP Ann.* 67(1): 409–412. <https://doi.org/10.1016/j.cirp.2018.04.109>.
- Voormeeren, S. 2012. Dynamic substructuring methodologies for integrated dynamic analysis of wind turbines. Ph.D. thesis, Precision and Microsystem Engineering, Section Engineering Dynamics, TU Delft. <https://doi.org/10.4233/uuid:f45f0548-d5ec-46aa-be7e-7f1c2b57590d>.
- Antoulas, A.C. 2005. *Approximation of Large-Scale Dynamical Systems*. Adv. Des. Control, 6. SIAM Publications: Philadelphia. <https://doi.org/10.1137/1.9780898718713>.
- Baur, U., P. Benner and L. Feng. 2014. Model order reduction for linear and nonlinear systems: A system-theoretic perspective. *Arch. Comput. Methods Eng.* 21(4): 331–358. <https://doi.org/10.1007/s11831-014-9111-2>.
- Antoulas, A.C., C.A. Beattie and S. Güğercin. 2020. *Interpolatory Methods for Model Reduction, Computational Science and Engineering*. SIAM Publications, Philadelphia. <https://doi.org/10.1137/1.9781611976083.fm>.
- Benner, P., S. Grivet-Talocia, A. Quarteroni, G. Rozza, W.H.A. Schilders and L.M. Silveira (eds). 2021. *Model Order Reduction. Volume 1: System- and Data-Driven Methods and Algorithms*. De Gruyter, Berlin. <https://doi.org/10.1515/9783110498967>.
- Lutowska, A. 2012. Model order reduction for coupled systems using low-rank approximations. Ph. D. thesis, Department of Mathematics and Computer Science, Eindhoven University of Technology. <https://doi.org/10.6100/IR729804>.
- Vandendorpe, A. and P. Van Dooren. 2008. Model reduction of interconnected systems. In: (W.H.A. Schilders, H.A. van der Vorst and J. Rommes, eds) *Model Order Reduction: Theory, Research Aspects and Applications*. Springer, Berlin, Heidelberg, pp. 305–321. https://doi.org/10.1007/978-3-540-78841-6_14.
- Schneider, A. and P. Benner. 2017. Reduced representation of power grid models. In: (P. Benner, ed) *System Reduction for Nanoscale IC Design, Mathematics in Industry*. Springer. https://doi.org/10.1007/978-3-319-07236-4_3.
- Benner, P. and L. Feng. 2015. Model order reduction for coupled problems (survey). *Appl. Comput. Math.* 14(1): 3–22. <http://acmij.az/view.php?lang=az&menu=journal&id=372>.
- Cruz Varona, M., R. Gebhart, J. Suk and B. Lohmann. 2019. Practicable simulation-free model order reduction by nonlinear moment matching. <http://arxiv.org/abs/1901.10750>.
- Benner, P. and T. Stykel. 2017. Model order reduction for differential-algebraic equations: A survey. In (A. Ilchmann and T. Reis, eds) *Surveys in Differential-Algebraic Equations IV, Differential-Algebraic Equations Forum*. Springer, Cham, pp. 107–160. https://doi.org/10.1007/978-3-319-46618-7_3.
- Lang, N., J. Saak and P. Benner. 2014. Model order reduction for systems with moving loads. *Automatisierungstechnik* 62(7): 512–522. <https://doi.org/10.1515/auto-2014-1095>.
- Benner, P. 2009. Modellordnungsreduktion für strukturmechanische FEM-Modelle von Werkzeugmaschinen. Project Report, TU Chemnitz. <https://nbn-resolving.org/urn:nbn:de:bsz:ch1-200901725>.
- Fehr, J. 2011. Automated and error controlled model reduction in elastic multibody systems. Ph. D. Thesis, Universität Stuttgart.
- Holzwarth, P. 2017. Modellordnungsreduktion für substrukturierte mechanische systeme. In (P. Eberhard, ed) *Schriften aus dem Institut für Technische und Numerische Mechanik der Universität Stuttgart* 51. Shaker Verlag, Aachen (in german).
- Benner, P., M. Köhler and J. Saak. 2021. Matrix equations, sparse solvers: M-M.E.S.S.-2.0.1 – philosophy, features and application for (parametric) model order reduction. In: (P. Benner, T. Breiten, H. Faßbender, M. Hinze, T. Stykel and R. Zimmermann, eds) *Model Reduction of Complex*

Dynamical Systems. International Series of Numerical Mathematics 171. Birkhäuser, Cham. pp. 369–392. https://doi.org/10.1007/978-3-030-72983-7_18.

28. Vettermann, J., J. Saak and A. Steinert. 2022. Code and data for numerical experiments in “compact thermo-mechanical models for the fast simulation of machine tools with nonlinear component behavior”. <https://doi.org/10.5281/zenodo.6778458>.
29. Cruz Varona, M. and B. Lohmann. 2017. Model reduction of linear time-varying systems with applications for moving loads. In (P. Benner, M. Ohlberger, A. Patera, G. Rozza and K. Urban, eds) *Model Reduction of Parametrized Systems*. Springer, Cham, pp. 367–386. https://doi.org/10.1007/978-3-319-58786-8_23.

Bionotes



Julia Vettermann
Faculty of Mathematics, Technische Universität Chemnitz, Reichenhainer Straße 39/41, 09126 Chemnitz, Germany
julia.vettermann@mathematik.tu-chemnitz.de

Julia Vettermann has studied industrial mathematics at the Technische Universität Chemnitz and afterwards joined the research group Mathematics in Industry and Technology of Prof. Dr. Peter Benner. Her research interests include all aspects of (parametric) model order reduction in the field of machine tool models.



Alexander Steinert
Laboratory for Machine Tools and Production Engineering (WZL), RWTH Aachen University, Steinbachstraße 19, 52074 Aachen, Germany
a.steinert@wzl.rwth-aachen.de

Alexander Steinert has studied mechanical engineering (B.Sc.) and production engineering (M.Sc.) at RWTH Aachen University. After his graduation in 2018, he entered WZL as research assistant in the field of thermal effects in machine tools. Since 2021, Alexander Steinert has been the leader of the group Machine Investigation and Evaluation at WZL.



Christian Brecher
Laboratory for Machine Tools and Production Engineering (WZL), RWTH Aachen University, Steinbachstraße 19, 52074 Aachen, Germany
c.brecher@wzl.rwth-aachen.de

After finishing his academic studies in mechanical engineering, Christian Brecher started his professional career first as a research assistant and later as team leader in the group Machine Investigation and Evaluation at WZL. From 1999 to 2001, he was responsible for the department of Machine Technology in his capacity as chief engineer.

After a short spell as a consultant in the aviation industry, in 2001 Christian Brecher was appointed as director for development at DS Technologie Werkzeugmaschinenbau GmbH, Mönchengladbach, where he carried the responsibility for construction and development until 2003.

Since January 1, 2004, Christian Brecher has been ordinary professor for Machine Tools at the Laboratory for Machine Tools and Production Engineering (WZL) of the RWTH Aachen as well as the director of the Department for Production Machines at the Fraunhofer Institute for Production Technology IPT. On January 1, 2018, Christian Brecher has been appointed the executive director of Fraunhofer IPT.

Christian Brecher is spokesperson and CEO of the RWTH Cluster of Excellence Internet of Production (IoP).

His research interests cover the fields of metrological investigation, calculation, and optimization of production machines, drive technology, robotics, machine data analytics and NC technology, automation technology, and gear technology.



Peter Benner
Computational Methods in Systems and Control Theory, Max Planck Institute for Dynamics of Complex Technical Systems, Sandtorstraße 1, 39106 Magdeburg, Germany
benner@mpi-magdeburg.mpg.de

Peter Benner received the Diploma in mathematics from the RWTH Aachen University, Aachen, Germany, in 1993. From 1993 to 1997, he worked toward the Ph.D. at the University of Kansas, Lawrence, KS, USA, and the TU Chemnitz-Zwickau, Germany, where he received the Ph.D. in Mathematics in February 1997. In 2001, he obtained the Habilitation (Venia Legendi) in Mathematics from the University of Bremen, Germany. He was an Assistant Professor with the University of Bremen, Germany, from 1997 to 2001. After spending a term as Visiting Associate Professor with the TU Hamburg-Harburg, Germany, he was a Lecturer in Mathematics with the TU Berlin, Germany, from 2001 to 2003. Since 2003, he has been a Professor for Mathematics in Industry and Technology with the TU Chemnitz. In 2010, he was appointed as one of the four Directors of the Max Planck Institute for Dynamics of Complex Technical Systems, Magdeburg, Germany. Since 2011, he has also been an Honorary Professor

with the Otto-von-Guericke University of Magdeburg, Germany. He is a SIAM Fellow (Class of 2017).

His research interests include scientific computing, numerical mathematics, systems theory, and optimal control. A particular emphasis has been on applying methods from numerical linear algebra and matrix theory in systems and control theory. Recent research focuses on numerical methods for optimal control of systems modeled by evolution equations (PDEs, DAEs, SPDEs), model order reduction, preconditioning in optimal control and UQ problems, and Krylov subspace methods for structured or quadratic eigenproblems. Research in all these areas is accompanied by the development of algorithms and mathematical software suitable for modern and high-performance computer architectures.

**Jens Saak**

Computational Methods in Systems and Control Theory, Max Planck Institute for Dynamics of Complex Technical Systems, Sandtorstraße 1, 39106 Magdeburg, Germany

saak@mpi-magdeburg.mpg.de

Jens Saak has studied industrial mathematics at the Zentrum für Technomathematik (ZeTeM) at University of Bremen until 2003. He then moved to the Department of Mathematics of TU Chemnitz, joining the Mathematics in Industry and Technology group (Prof. Dr. Peter Benner), where he received his PhD in 2009. In 2010 Jens joined Prof. Benner moving to the Max Planck Institute for Dynamics of Complex Technical Systems, where he has headed the Teams on “Scientific Computing” (2010–2020) and “Matrix Equations” (2013–2020) and got appointed Team Leader of the new Team “Data, Infrastructure, Software & Computing” in the department for Computational Methods in Systems and Control Theory in 2021. His main interest are fast, efficient, accurate and high performance implementations of solvers for algebraic and differential matrix equations and their applications in control and model order reduction of large-scale systems, driven by partial differential equations, especially in the context of demanding industrial and (mechanical) engineering environments.